



Optics Letters

Experimental demonstration of dynamic spatiotemporal structured beams that simultaneously exhibit two orbital angular momenta by combining multiple frequency lines, each carrying multiple Laguerre–Gaussian modes

KAI PANG,^{1,*} KAIHENG ZOU,¹ ZHE ZHAO,¹ HAO SONG,¹ YIYU ZHOU,² MAXIM KARPOV,³ MURAT YESSENOV,⁴ ABBAS SHIRI,⁴ HAOQIAN SONG,¹ RUNZHOU ZHANG,¹ HUIBIN ZHOU,¹ XINZHOU SU,¹ NANZHE HU,¹ AMIR MINOOFAR,¹ TOBIAS J. KIPPENBERG,³ ROBERT W. BOYD,^{2,5} AYMAN F. ABOURADDY,⁴ MOSHE TUR,⁶ AND ALAN E. WILLNER¹

¹Department of Electrical and Computer Engineering, University of Southern California, Los Angeles, California 90089, USA

²The Institute of Optics, University of Rochester, Rochester, New York 14627, USA

³École Polytechnique Fédérale de Lausanne (EPFL), Lausanne, Switzerland

⁴CREOL, The College of Optics & Photonics, University of Central Florida, Orlando, Florida 32816, USA

⁵Department of Physics and Astronomy, University of Ottawa, Ottawa, Ontario, Canada

⁶School of Electrical Engineering, Tel Aviv University, Ramat Aviv 69978, Israel

*Corresponding author: kaipang@usc.edu

Received 6 June 2022; revised 21 July 2022; accepted 22 July 2022; posted 22 July 2022; published 4 August 2022

In general, there are different, relatively independent forms of orbital angular momenta at a given propagation distance, which might exhibit different dynamic spatial characteristics. One type involves a beam with a helical phasefront that rotates around its own beam center, such as a Laguerre–Gaussian (LG) beam with an azimuthal index not equal to zero. The other one is a Gaussian-like beam dot that revolves around a central axis. Here, we experimentally demonstrate the generation of a dynamic spatiotemporal (ST) structured beam that simultaneously exhibits both rotation and revolution at a given propagation distance. Nine Kerr frequency comb lines are coherently combined, each carrying a designed superposition of multiple LG modes containing one unique ℓ value and multiple p values. Experimental results show that the mode purity of the reconstructed revolving and rotating LG₃₀ beam is ~89% when both the beam waist and revolving radius (R) are 0.4 mm. Moreover, we explore the effects of the number of frequency comb lines and the R value on the mode purity of the generated ST beam. Consequently, we find that a higher mode purity can be achieved by involving more frequency comb lines or reducing the R. © 2022 Optica Publishing Group

<https://doi.org/10.1364/OL.466058>

Structured light has gained increasing interest due to the novel amplitude/phase spatial distributions that can be achieved and used in various applications [1–6]. Recently, structured beams carrying orbital angular momentum have attracted interest [7–9]. In general, there are different, relatively independent, forms of

orbital angular momenta at a given propagation distance, which might exhibit different dynamic spatial characteristics [10]. One type involves a beam with a helical phasefront that rotates around its own beam center, such as a Laguerre–Gaussian beam with an azimuthal index not equal to zero [7,8,11]. A second form of orbital angular momentum is a Gaussian-like beam dot that revolves around a central axis (i.e., revolution) [12,13]. Indeed, this is analogous to the Earth, which exhibits both rotation around its own axis and revolution around the Sun.

In general, a beam at a given propagating distance from a transmitter can be tailored using coherent interference to exhibit nearly any fixed spatial distribution by using a complex-weighted combination of multiple spatial modes from a complete 2-dimensional (2D) LG modal basis set located at a single optical frequency [14,15]. It should be noted that LG modes can be characterized by two modal indices, ℓ and p , in which ℓ is the number of 2π phase shifts in the azimuthal direction and $p + 1$ is the number of concentric intensity vortex rings [11].

Moreover, it was recently shown by theory and simulation that a dynamic spatiotemporal (ST) light beam can be generated that simultaneously exhibits rotation and revolution at a given propagation distance [16]. This scenario is enabled by combining multiple optical frequency comb lines [17], with each line carrying a superposition of multiple LG _{ℓ,p} modes containing a unique ℓ value and multiple p values. The frequency spacing of the comb lines introduces a time-varying relative phase delay $\Delta\varphi(t)$ between the LG _{ℓ,p} modes on neighboring frequencies. Consequently, the $\Delta\varphi(t)$ leads to time-dependent constructive and destructive interference between all the LG _{ℓ,p} modes on different frequencies, which produces a dynamically revolving

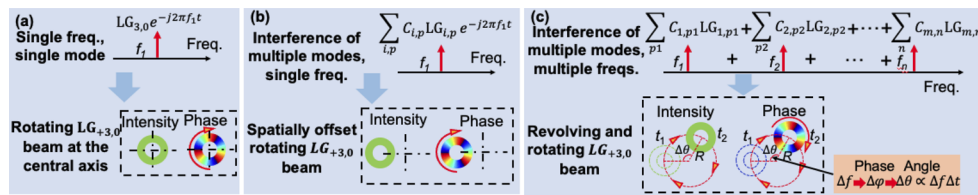


Fig. 1. (a) When a single frequency line carries a single LG mode, a rotating LG beam at the central axis is generated. (b) When a single frequency line carries multiple LG modes, a spatially offset rotating LG beam can be generated. (c) When multiple frequency lines—each carrying a superposition of multiple LG modes containing one unique ℓ value and multiple p values—are combined, a revolving and rotating LG beam is generated. Δf is the frequency space; $\Delta\theta$ is the revolving angle; Δt is the temporal delay; R is the revolving radius; $C_{i,j}$ are the complex coefficients.

and rotating LG beam [16]. ST beams exhibiting two types of orbital angular momenta might be potentially used for various applications, such as optical sensing [18,19]. In this scenario, the dynamic characteristics of this ST beam with multiple frequencies might help us to dynamically take multiple measurements of various object parameters [18,19].

In this paper, we experimentally demonstrate the generation of this dynamic ST beam that exhibits both rotation and revolution at a given distance using a Kerr frequency comb [20]. Nine frequencies are coherently combined, each carrying a superposition of LG modes with one unique ℓ value and multiple p values. Experimental results show that the mode purity of the revolving and rotating LG₃₀ beam is $\sim 89\%$ when both the beam waist and revolving radius (R) are 0.4 mm. Moreover, we explore the effects of the number of frequency lines and R value on the mode purity of the generated ST beam. Consequently, we find that a higher mode purity can be achieved by involving more frequency comb lines or reducing the R .

Figure 1 illustrates the concept of the generation of a dynamically revolving and rotating LG $_{\ell,p}$ beam. In general, when a single frequency carries a single LG $_{\ell,p}$ mode, the generated beam has a ring-like intensity profile, as shown in Fig. 1(a). In addition, it also has a twisting phasefront of $\exp(j\ell\phi)$, which leads to a non-zero Poynting vector in the azimuthal direction. Such a Poynting vector indicates that the phasefront of the beam rotates around its beam center over time. In general, a beam with a given spatial distribution can be produced by a coherent combination of multiple modes from a complete spatial modal basis set at a single frequency [7,8]. Therefore, by designing the complex weight of each LG $_{\ell,p}$ mode, a rotating beam with a designed offset could be generated due to their interference. The complex coefficients of LG $_{\ell,p}$ mode components can be obtained by decomposing such an offset beam into the LG $_{\ell,p}$ modal basis set. Since all the LG $_{\ell,p}$ modes are located on a single frequency, the relative phase delay between these modes remain the same, leading to a “static” intensity profile.

Previous work has shown that the beam position in the azimuthal direction can be controlled by tuning the relative phase delay $\Delta\phi(t)$ between neighboring LG modes (i.e., $\Delta\ell = 1$) that are used for the beam generation [21]. Since ℓ represents the number of 2π phase shifts, such a $\Delta\phi(t)$ would induce a change in the condition of constructive interference in the azimuthal direction, leading to a change in the azimuthal position of the beam. One potential method to further introduce dynamic revolution to the offset LG beam is to add a time-variant $\Delta\phi(t)$ among the neighboring LG modes, as shown in Fig. 1(c). This could be achieved by using multiple frequency lines with a spacing of Δf , each carrying LG $_{\ell,p}$ modes with a unique ℓ and multiple

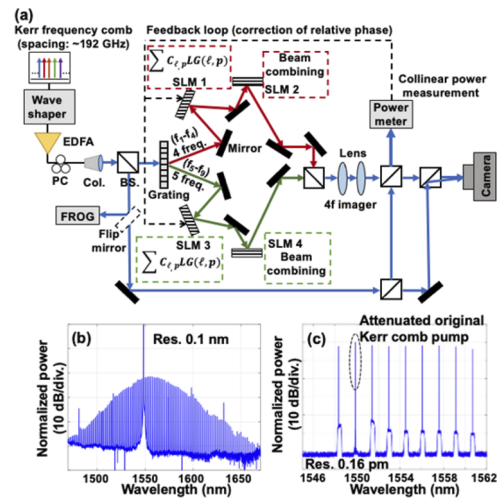


Fig. 2. Experimental setup for the generation and detection of ST beams. EDFA: erbium-doped fiber amplifier; PC: polarization controller; Col.: collimator; FROG: frequency-resolved optical gating; SLM: spatial light modulator; BS: beam splitter. Optical spectra of (b) Kerr frequency comb and (c) selected nine frequency lines after the waveshaper.

p values [16]. Consequently, a $\Delta\phi(t) = 2\pi\Delta f t$ between neighboring LG modes is introduced, and the generated LG $_{\ell,p}$ beam revolves around the central axis with time.

Figure 2(a) shows the experimental setup for the generation and detection of ST beams. A Kerr frequency comb source with a spacing of ~ 192 GHz is used, as shown in Fig. 2(b). Nine frequency lines are selected by a waveshaper, as shown in Fig. 2(c). The output is amplified and then sent into a collimator that generates a collimated Gaussian beam. Subsequently, the incoming beam is split into two branches by a beam splitter (BS). One is used as a reference beam, and the relative phase of the nine frequency lines is measured using a frequency-resolved optical gating (FROG), such that their relative phase is tuned to be zero by the waveshaper, which means they are in phase. The other branch is sent to a diffraction grating. Consequently, the frequencies are spatially separated and directed to different positions on spatial light modulators (SLMs) 1 and 3. Different phase holograms are loaded at these positions to create specific beams composed of multiple LG modes for different frequency lines. In our experiment, the nine frequencies are split into two groups, each of which is spatially modulated by a single SLM. This splitting is done mainly to ensure high modal purity of each LG beam. Given the limited effective area of

our SLMs, this grouping enables there to be enough pixels on each SLM to operate at each frequency. It should be noted that by using an SLM with a larger effective area, it is possible to use only one SLM to shape all nine frequencies [22]. Furthermore, there are other methods that could be used to efficiently perform spatial modulation and beam combining, such as low-loss multi-plane light converters (MPLC) [23] and Dammann gratings [24]. Subsequently, these resulting beams at different frequencies are combined using another two SLMs (SLM 2, 4) and a BS. The phase patterns on SLMs 2 and 4 are combinations (i.e., superpositions) of multiple grating designs. The period and direction of each grating pattern are tuned to control the output direction of each frequency. Consequently, the nine frequencies have the same output direction and are coherently combined. At the receiver, two lenses are utilized as a $4f$ imaging system, which images all the beams from SLM 1 and 3 to the camera to achieve a high mode purity, which decreases with the propagation distance [16]. Subsequently, three BSs are used to split the generated beam and the reference beam into two branches and combine them in two ways. On the one hand, the two beams are collinearly combined for power measurement for the correction of their relative phase. On the other hand, they are combined with a small angle for off-axis holography using a camera [25]. Here, the theoretical revolving period is ~ 5.2 ps since the spacing of frequency comb lines is 192 GHz.

To generate and detect the LG_{30} beam with an R and a beam waist of 0.4 mm, the process includes the following steps. (i) The coefficients of all the LG modes are determined by the decomposition of the ST beam in a simulation based on the theoretical study in Ref. [16]. Figures 3(a1) and 3(a2) present the simulated amplitudes and phases of the complex coefficients of all LG modes used for generation. It should be noted that

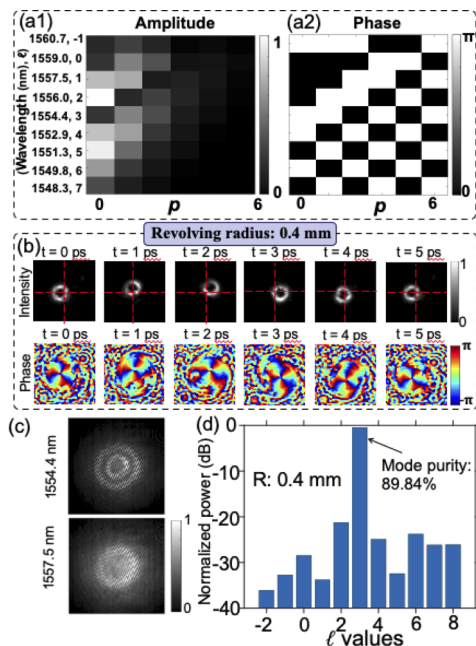


Fig. 3. (a) Designed complex coefficients of all LG modes used for the generation of a revolving and rotating LG_{30} beam with an R and beam waist of 0.4 mm. (b) Experimental intensity and phase profiles of such a beam. (c) Raw frames captured by the camera of the interference between the reference beam and wavelengths of 1554.4 nm and 1557.5 nm. (d) Power distribution of beams with different ℓ values.

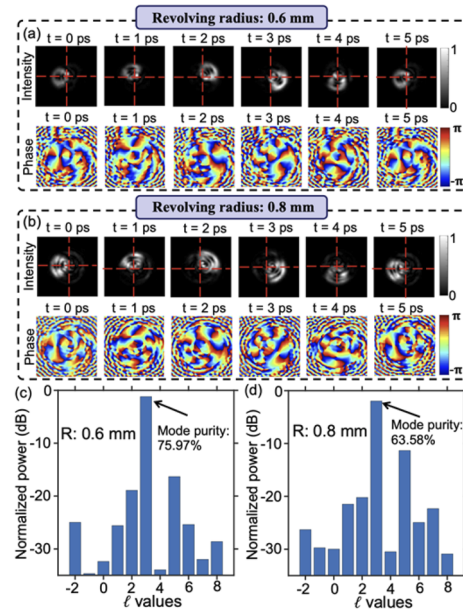


Fig. 4. Experimental intensity and phase profiles of revolving and rotating LG_{30} beams with a beam waist of 0.4 mm and R values of (a) 0.6 and (b) 0.8 mm, respectively. (c) Power distributions of light beams with different ℓ values and R values of (c) 0.6 and (d) 0.8 mm, respectively.

both the phases and amplitudes of the LG modes should be controlled, which is achieved in our experimental setup by using “phase-only” SLMs [Fig. 3(a)]. We note that amplitude control of the LG modes is achieved by designing the grating pattern of our SLMs, in which the diffraction efficiency (i.e., power efficiency in a given direction) of various spatial locations of a given LG mode is tuned according to the desired amplitude [26]. (ii) Based on the simulated coefficients of the LG modes, specific phase patterns are constructed on the SLMs to generate a beam comprising LG modes with a specific ℓ but multiple p values using the method described in [27]. (iii) At the receiver, the spatial amplitude and phase profiles for each frequency are retrieved using off-axis holography. Subsequently, the ST beam is reconstructed by numerically combining all the frequencies. Figure 3(b) presents the intensity and phase profiles of the reconstructed revolving and rotating LG_{30} beam over time at a given distance (in this case, the distance is zero from the output aperture). The dynamic helical phasefront and amplitude profiles indicate both dynamic rotation and revolution over time. Therefore, we find that the beam revolves around a central axis and has almost performed a complete revolution. Figure 3(c) shows the raw frames captured by the camera of the interference between the reference beam and the wavelengths of 1554.4 nm and 1557.5 nm. The frequency lines of the generated ST beam and the reference beam are filtered by adjusting the waveshaper. Figure 3(d) presents the power distribution of light beams with different ℓ values. These values for different $LG_{\ell,0}$ modes can be obtained using $P_{\ell} = \left| \iint E_{\ell}(x, y) E_2^*(x, y) dt \right|^2$, where $E_{\ell}(x, y)$ is the normalized reconstructed electric field of the generated ST beam and $E_2(x, y)$ is the normalized electric field of a conventional $LG_{\ell,0}$ beam with a center that overlaps with the generated beam [16]. It is observed that the obtained mode purity is 89.84%.

In addition, using these nine frequencies, we also investigate the generation of these ST beams with different R values.

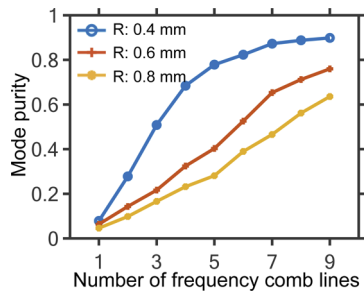


Fig. 5. (a) The mode purity of the ST beam when using different numbers of frequency lines and an R value of 0.4, 0.6, or 0.8 mm.

Figures 4(a) and 4(b) show the intensity and phase profiles of a reconstructed revolving and rotating LG_{30} beam with a beam waist of 0.4 mm and an R value of (a) 0.6 and (b) 0.8 mm, respectively. This shows that, compared to the case of $R = 0.4$ mm, the generated ST beam is somewhat distorted when using the same set of frequency lines for a large R value (0.6 or 0.8 mm). As a result, the mode purity of the ST beam is 75.97% and 63.58% when R is 0.6 and 0.8 mm, respectively, as shown in Figs. 4(c) and 4(d). This might be because the azimuthal mode will be spatially distributed within a smaller azimuthal range as the R of the ST beam increases. As a result, the number of comb lines that are required for a high mode purity also increases after applying a Fourier transformation from the azimuthal spatial domain to the frequency domain [16]. As mentioned above, multiple LG modes can be used to generate a single-frequency LG beam with a spatial offset [21]. However, as the spatial offset increases, the mode purity of the generated single-frequency LG beam will be reduced given the superposition of the same set of LG modes. This could be due to the fact that the spatial dimension in the azimuthal direction of the beam becomes smaller when the spatial offset is larger; this may necessitate more LG modes with a wider azimuthal index (i.e., ℓ) range to maintain a high modal purity [21]. As expected, when the number of the frequencies used for the generation of the ST beam decreases, the mode purity of the desired LG beam also decreases, as shown in Fig. 5. Theoretically, LG modes with different modal indices are orthogonal to each other, which can ensure little inherent modal coupling between different LG modes. In general, the higher the mode purity of an LG mode, the lower the modal coupling to other LG modes. This might be important in some applications, such as optical sensing using multiple LG modes [19]. Moreover, in addition to the revolving radius and the number of comb lines used, another issue that might affect the mode purity of the generated LG beam is the pixel size of the SLM [8].

Funding. Qualcomm Innovation Fellowship (QIF); Office of Naval Research through a MURI award (N00014-20-1-2789); Vannevar Bush Faculty Fellowship Sponsored by the Basic Research Office of the Assistant Secretary of Defense (ASD) for Research and Engineering (R&E) and Funded by the Office of Naval Research (ONR) (N00014-16-1-2813).

Disclosures. The authors declare no conflicts of interest.

Data availability. Data underlying the results presented in this paper are not publicly available at this time but may be obtained from the authors upon reasonable request.

REFERENCES

- B. Sun, P. S. Salter, C. Roeder, A. Jesacher, J. Strauss, J. Heberle, M. Schmidt, and M. J. Booth, *Light: Sci. Appl.* **7**, 17117 (2018).
- L. J. Wang, A. Kuzmich, and A. Dogariu, *Nature* **406**, 277 (2000).
- H. E. Kondakci and A. F. Abouraddy, *Nat. Photonics* **11**, 733 (2017).
- K. Dholakia and T. Čižmár, *Nat. Photonics* **5**, 335 (2011).
- L. G. Wright, D. N. Christodoulides, and F. W. Wise, *Science* **358**, 94 (2017).
- M. Yessenov, B. Bhaduri, H. E. Kondakci, and A. F. Abouraddy, *Opt. Photonics News* **30**, 34 (2019).
- L. Allen, M. W. Beijersbergen, R. J. C. Spreeuw, and J. P. Woerdman, *Phys. Rev. A* **45**, 8185 (1992).
- A. Yao and M. J. Padgett, *Adv. Opt. Photonics* **3**, 161 (2011).
- N. Jhaji, I. Larkin, E. W. Rosenthal, S. Zahedpour, J. K. Wahlstrand, and H. M. Milchberg, *Phys. Rev. X* **6**, 031037 (2016).
- J. Zhao, I. D. Chremmos, D. Song, D. N. Christodoulides, N. K. Efremidis, and Z. Chen, *Sci. Rep.* **5**, 12086 (2015).
- R. L. Phillips and L. C. Andrews, *Appl. Opt.* **22**, 643 (1983).
- G. Pariente and F. Quéré, *Opt. Lett.* **40**, 2037 (2015).
- C. Haug and F. Dabby, *IEEE J. Quantum Electron.* **7**, 489 (1971).
- C. Schulze, A. Dudley, D. Flamm, M. Duparré, and A. Forbes, *New J. Phys.* **15**, 073025 (2013).
- T. Kaiser, D. Flamm, S. Schröter, and M. Duparré, *Opt. Express* **17**, 9347 (2009).
- Z. Zhao, H. Song, R. Zhang, K. Pang, C. Liu, H. Song, A. Almainan, K. Manukyan, H. Zhou, B. Lynn, R. W. Boyd, M. Tur, and A. E. Willner, *Nat. Commun.* **11**, 1 (2020).
- P. Del'Haye, A. Schliesser, O. Arcizet, T. Wilken, R. Holzwarth, and T. J. Kippenberg, *Nature* **450**, 1214 (2007).
- S. Berg-Johansen, F. Töppel, B. Stiller, P. Banzer, M. Ornigotti, E. Giacobino, G. Leuchs, A. Aiello, and C. Marquardt, *Optica* **2**, 864 (2015).
- G. Xie, H. Song, Z. Zhao, G. Millione, Y. Ren, C. Liu, R. Zhang, C. Bao, L. Li, Z. Wang, K. Pang, D. Starodubov, B. Lynn, M. Tur, and A. E. Willner, *Opt. Lett.* **42**, 4482 (2017).
- K. Pang, K. Zou, Z. Zhao, H. Song, Y. Zhou, M. Karpov, M. Yessenov, A. Shirir, H. Song, R. Zhang, H. Zhou, X. Su, N. Hu, A. Minoofar, T. J. Kippenberg, R. W. Boyd, A. F. Abouraddy, M. Tur, and A. E. Willner, in *Conference on Lasers and Electro-Optics (CLEO) 2021*, paper STu1D.1 (2021).
- G. Xie, C. Liu, L. Li, Y. Ren, Z. Zhao, Y. Yan, N. Ahmed, Z. Wang, A. J. Willner, C. Bao, Y. Cao, P. Liao, M. Ziyadi, A. Almainan, S. Ashrafi, M. Tur, and A. E. Willner, *Opt. Lett.* **42**, 991 (2017).
- X. Yang, P. Song, H. Zhang, and Q.-H. Wang, *Opt. Express* **27**, 38236 (2019).
- N. K. Fontaine, R. Ryf, H. Chen, D. T. Neilson, K. Kim, and J. Carpenter, *Nat. Commun.* **10**, 1865 (2019).
- T. Lei, M. Zhang, Y. Li, P. Jia, G. N. Liu, X. Xu, Z. Li, C. Min, J. Lin, C. Yu, H. Niu, and X. Yuan, *Light: Sci. Appl.* **4**, e257 (2015).
- Y. Zhou, J. Zhao, B. Braverman, K. Pang, R. Zhang, A. E. Willner, Z. Shi, and R. W. Boyd, *Phys. Rev. Appl.* **15**, 034011 (2021).
- T. Ando, Y. Ohtake, N. Matsumoto, T. Inoue, and N. Fukuchi, *Opt. Lett.* **34**, 34 (2009).
- K. Pang, H. Song, X. Su, K. Zou, Z. Zhao, H. Song, A. Almainan, R. Zhang, C. Liu, N. Hu, S. Zach, N. Cohen, B. Lynn, A. F. Molisch, R. W. Boyd, M. Tur, and A. E. Willner, *Opt. Lett.* **45**, 6310 (2020).